Science and Technology Indonesia
e-ISSN:2580-4391 *p*-ISSN:2580-4405
Vol. 9, No. 2, April 2024

Research Paper

Fabrication and Optimization of Primary Batteries Using Ni/Graphene Nanosheet Electrodes

Kerista Tarigan[1*], Rikson Siburian[2], Erika Arta Mevia Sitorus[2], Frikson Jony Purba[3], Yosia Gopas Oetama Manik[4]

[1]*Department of Physics, Faculty of Mathematics and Natural Sciences, Universitas Sumatera Utara, Medan, Sumatera Utara, 20155, Indonesia*
[2]*Department of Chemistry, Faculty of Mathematics and Natural Sciences, Universitas Sumatera Utara, Medan, Sumatera Utara, 20155, Indonesia*
[3]*Department of Elementary School Teacher Education, Faculty of Teacher Training and Education, Universitas Quality, Medan, Sumatera Utara, 20132, Indonesia*
[4]*Postgraduate of Chemistry Department, Universitas Sumatera Utara, FMIPA–USU, Medan, Sumatera Utara, 20155, Indonesia*
***Corresponding author**: kerista@usu.ac.id

Abstract
This study aims to investigate the impact of varying the mass ratio of Ni to Graphene Nano Sheets (GNS) and how incorporating GNS affects the performance of a primary battery prototype (Ni/GNS//electrolyte//GNS). The primary battery prototype was developed using both impregnation and alloy methods. Different mass ratios of Ni/GNS to electrolyte to GNS were tested, including ratios of 1:2:1 (A), 2:2:1 (B), 1:2:2 (C), 2:1:2 (D), and 1:1:2 (E). The characterization of GNS, Ni/GNS, and the primary battery prototype involved using X-Ray Diffraction (XRD) and Scanning Electron Microscope-Energy Dispersive X-Ray (SEM-EDX) instruments. A multimeter was employed to measure electrical conductivity, energy density, and power density. A potentiostat/galvanostat was used to measure cyclic voltammetry (CV) and electrochemical impedance spectroscopy (EIS). XRD analysis showed a broad and weak peak at $2\theta = 24.32°$ for GNS, confirming its successful synthesis. Additionally, a peak at $2\theta = 43.5°$ indicated effective deposition of Ni on the GNS surface in Ni/GNS. The SEM-EDX results supported the XRD findings, showing regularly spaced pores and a thin surface layer in GNS. Notably, white spots on the graphene surface in Ni/GNS indicated successful Ni deposition. In terms of electrical conductivity, the highest value was observed in the primary battery prototype for sample D (2:1:2), which measured 1.11 S/cm^2. These results were also supported by measurements of energy density and power density in sample D, which achieved the highest values among all samples, with 144,788 Wh/kg and 252,500 W/kg, respectively. Moreover, the CV and EIS measurements remained stable at 0.30 kΩ and 0.88 kΩ, suggesting that GNS could potentially conduct electrons owing to its electrical conductivity.

Keywords
Electrical Conductivity, Electrode, Ni/GNS, Primary Battery

Received: 10 December 2023, Accepted: 3 March 2024
https://doi.org/10.26554/sti.2024.9.2.413-426

1. INTRODUCTION

Batteries are energy devices with diverse energy or power export properties that are highly demanded to sustain a wide range of electrical facilities, from electromagnetic pulse equipment to vital hybrid/plug-in electrical devices (Chang et al., 2021) Batteries that possess high energy density, large capacity, stability, and affordability are highly sought after. There is significant societal interest in the research and advancement of rechargeable batteries due to their ability to be reused numerous times, resulting in lower ownership costs compared to primary batteries. However, it is important to acknowledge that rechargeable batteries may not always be suitable, such as in environments where recharging is impractical, like in remote mountain areas or underwater. In such situations, primary batteries are preferable due to their extended shelf life and high energy density. Additionally, primary batteries serve as crucial backup power sources for essential facilities like schools and hospitals. Therefore, it's imperative to also focus on finding economically viable primary batteries that pose no harm to the environment.

Primary batteries are easy to use and affordable, making them widely used in everyday life. Primary batteries generally consist of an anode (Zn), electrolyte (NH_4Cl and MnO_2), and cathode (graphite) (Moulai et al., 2020; Siburian and Silitonga, 2022; Wei et al., 2021). Previous research, experimenting with various ratios of battery components such as a Cu anode, NH_4Cl electrolyte, and graphene nanosheets (GNS) cathode, has yielded promising results for the development of future primary batteries (Siburian and Silitonga, 2022).

However, there are several issues that need to be addressed in the development of primary batteries, such as the complexity

of battery materials (Porzio and Scown, 2021), their relatively short lifespan (Hu et al., 2020), the efficiency of GNS production (Wan et al., 2020), and the potential scarcity of Lithium (Alessia et al., 2021) and Nickel as an anode material (Chang et al., 2021). A recent investigation into NiCo-MOF (metal organic frameworks) as an electrode reveals a capacity of 96.5 mAh/g at 2 mA/cm^2 at -40 °C, indicating an 85.2% capacity retention compared to that at 25 °C (An et al., 2024). While MOF demonstrates potential in enhancing reaction reversibility for Ni–Zn batteries, the adverse impact of the parasitic oxygen evolution reaction (OER) on the coulombic efficiency (CE) necessitates further control. Mechanistically, reducing the activity of water molecules and hydroxyl ions in the electrolyte is crucial for mitigating OER (Chang et al., 2021; An et al., 2024). Additionally, the freezing of electrolyte solutions at low temperatures significantly reduces ionic conductivity, leading to notable performance degradation (Lee et al., 2023; An et al., 2024).

Efforts have been made to tackle these problems, including the use of battery fuses to extend battery life (Reyes et al., 2018), the development of mass ratio comparisons in battery electrodes to achieve more efficient performance (Murata et al., 2019), and large-scale GNS production using pyrolysis methods that utilize coconut as a raw material (Siburian et al., 2023c). A recent study on GNS with resorcinol-formaldehyde has been reported. The porous GNS nanolayers facilitate ion transport, whereas the graphene networks enhance conductivity, thereby enhancing electron transport. As anticipated, the resultant porous carbon exhibits a substantial surface area of 690 m^2/g and achieves a notable specific capacitance of up to 324 F/g (Sun et al., 2022). However, previous research tends to analyze battery components only partially (Chen et al., 2021a; Chen et al., 2021b; Ha et al., 2022; Sayahpour et al., 2022; Zou et al., 2022). In addition, research on the use of Ni metal as an anode in primary batteries coupled GNS, considering the advantages of Ni's rust resistance and good electrical conductivity from GNS has been conducted (Siburian and Silitonga, 2022; Sun et al., 2022). As per a recent study, a novel electrode design strategy involves the controlled electrophoretic deposition of graphene onto the surface of the Ni-rich electrode. This process aims to enhance capacities and reduce the aging rate (Chameh et al., 2024). In addition, as is known, the strong interaction between Ni and GNS can result in more efficient electrical contact (Dahal and Batzill, 2014).

Despite progress in primary battery technology, there remains a significant research gap, particularly in addressing the complexity of battery materials, their limited lifespan, the efficiency of GNS production, and the looming scarcity of lithium for anodes. Current efforts, while valuable, often fail to provide a comprehensive analysis of these components and their interactions, leading to partial solutions that do not fully address the multifaceted challenges faced by the industry. Therefore, this study aims to investigate the optimization of a primary battery composed of Ni/GNS, NH_4Cl and MnO_2 electrolytes, and GNS. This research also compares the results of electrical conductivity analysis with several commercial primary batteries to demonstrate the advantages of the developed battery.

2. Experimental Section

2.1 Materials and Instrumentation

The materials used in this study are coconut shell (*Cocos nucifera L.*), activated carbon obtained from Sigma-Aldrich, and $NiCl_2{\cdot}6H_2O$ powder, MnO_2, NH_4Cl, and Al powder with analytical grade purchased from Merck. Glassware was used for the preparation of materials, and instruments like an Fourier Transform Infrared Spectroscopy (FTIR, Perkin Elmer Spectrum One), X-Ray Diffractometer (XRD, Rigaku PANanalytical), and Scanning Electron Microscope-Energy Dispersive X-Ray (SEM-EDX, JEOL Phenom) were employed for the characterization of the materials' structure and morphology. Furthermore, glass fuses, a digital multimeter (Sanwa), alligator clip cables, and a regulated DC power supply (Atten) were used for assessing the electrical conductivity of the materials. A potentiostat/galvanostat (Eco Chemie Autolab PGSTAT30, Netherlands), glassy carbon working electrode (GCE) with a diameter of 3 mm (Sigma-Aldrich), Ag/AgCl reference electrode (Thermo Scientific), platinum rod counter electrode (HY Electronic), and ultrasonication homogenizer (UH-650, B-One) were utilized for the electrochemical testing process.

2.2 Methods

2.2.1 Preparation of GNS

Five mature coconuts (*Cocos nucifera L.*) were cleaned of their fibers and wrapped in aluminum foil. They were then heated on a hot plate until cracking occurred. Subsequently, the coconut flesh was separated from the shell. The obtained coconut shells were pyrolyzed for 5 hours at a temperature of 600 °C to produce charcoal in chip form, which was then weighed along with activated carbon powder. Next, the mixture was placed in a furnace at 600 °C for 1 hour. It was then sieved using a 100-mesh screen to separate the coconut shell charcoal from the activated carbon. The coconut shells were washed with distilled water until clean and then dried in an oven at 105 °C. They were later characterized using FTIR, XRD and SEM-EDX (Siburian et al., 2022).

2.2.2 Preparation of 30% Ni-Coated GNS (%w/w)

A total of 0.5 g of GNS powder and 0.867 g of $NiCl_2{\cdot}6H_2O$ crystals were each mixed with 10 mL of ethanol and stirred for 1 hour to produce a mixture of GNS and Ni precursor solution. Then, the GNS mixture and Ni precursor solution were stirred for 3 hours to produce a Nickel-GNS mixture. The Nickel-GNS mixture was filtered using Whatman filter paper No. 42 to separate the filtrate and the precipitate. The obtained precipitate was dried at a temperature of 80 °C for 2 hours to produce a solid powder of 30% Ni/GNS, which was then characterized using FTIR, XRD and SEM-EDX (Manalu et al., 2022).

2.2.3 Electrolyte Preparation

The electrolyte, a key component of the primary battery, was prepared by separately dissolving 0.3 g of NH_4Cl and 0.3 g of MnO_2 in 10 mL of deionized water in separate beaker glasses.

2.2.4 Prototype Fabrication of Primary Batteries

A total of 0.3 g of GNS and 0.3 g of Ni/GNS were added to a glass beaker, followed by the addition of 10 mL of NH_4Cl solution and 10 mL of MnO_2 solution. A magnetic bar was placed into the glass beaker and the mixture was stirred for 6 hours. Subsequently, the two solutions were combined and stirred for 48 hours to produce a mixture of Ni/GNS//electrolyte//GNS. The Ni/GNS//electrolyte//GNS mixture was then filtered using Whatman No. 42 filter paper, resulting in filtrate and residue. The filtrate was not further processed. The obtained residue was dried at a temperature of 105 °C for 12 hours, yielding a solid powder. This solid powder was then weighed and characterized using FTIR, XRD, and SEM-EDX. This procedure was repeated for mass ratios of 1:2:1 (A); 2:2:1 (B); 1:2:2 (C); 2:1:2 (D); and 1:1:2 (E).

2.2.5 Electrical Conductivity Assay

A total of 0.25 g of Ni/GNS//electrolyte//GNS powder was placed into a glass fuse, compacted until full, and sealed with a fuse cap. Then, the fuse was connected with alligator clip cables to the negative and positive poles on a multimeter and regulated DC power supply circuit. Next, the regulated DC power supply was turned on, and the electrical conductivity of Ni/GNS//electrolyte//GNS was measured at voltages of 0.5, 1.0, and 1.5 V, and the current output (A) is recorded on the multimeter (Siburian and Silitonga, 2022). The electrical conductivity measurement was carried out using the same procedure on the electrode powder of the battery for all variations.

2.2.6 Electrochemical Analysis of GNS

Electrochemical measurements were performed using a potentiostat/galvanostat in a three-electrode system. The electrochemical cells comprised a modified glassy carbon working electrode (GCE, 3 mm diameter), an Ag/AgCl reference electrode, and a platinum rod counter electrode. The GCE was polished with alumina powder and rinsed thoroughly with distilled water prior to use. A 1 mg/mL GNS homogenized suspension was prepared by dispersing the synthesized GNS in distilled water through ultrasonication for 30 minutes. Subsequently, 5 μL of the suspension was drop-casted on the GCE surface and air-dried freely at ambient temperature, forming GNS/GCE. The prepared electrode was then analyzed using CV and EIS in a three-electrode system (Sookhakian et al., 2020).

3. RESULTS AND DISCUSSION

3.1 XRD Characterization of GNS and Ni/GNS

In this study, GNS derived from coconut shell were used as the cathode material, as part of an effort to replace graphite (the standard cathode material in commercial primary batteries). The production of GNS using the pyrolysis method presents several advantages over other methods. Notably, it does not require the use of graphite or strong acids. It is also cost-effective, abundant, simple, and environmentally friendly (Supeno and Siburian, 2020).

The characterization results of the GNS using XRD are displayed in Figure 1. This figure reveals a weak and broad peak at 2θ = 24.32°, which is characteristic of the GNS sheets. This peak corresponds to the reflection plane C (002), a major component of graphene. These findings align with the crystallographic data from JCPDS card no. 00–052–1907. Such a result indicates that the material comprises nano-sized particles that are stacked in the interlayer spaces of graphene (Krawczyk et al., 2019). This confirms that the GNS was successfully synthesized.

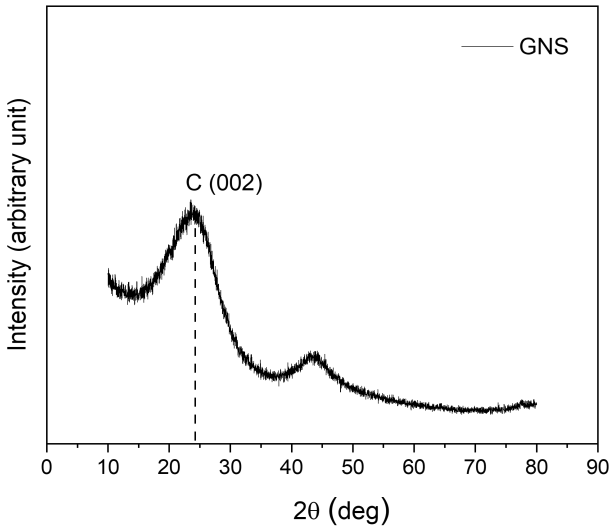

Figure 1. XRD Diffraction Pattern of GNS

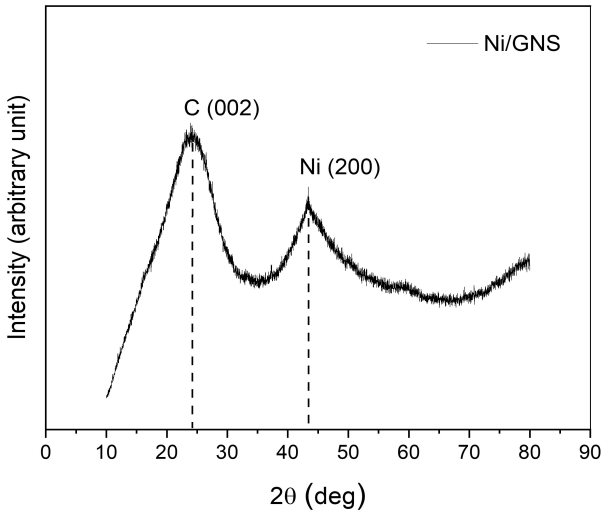

Figure 2. XRD Diffraction Pattern of Ni/GNS

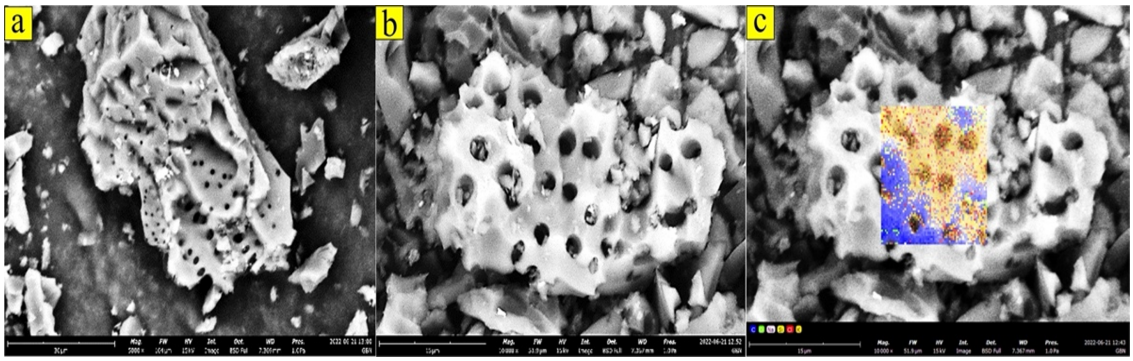

Figure 3. (a) GNS Morphology at 5000× Magnification, (b) GNS Morphology at 10,000× Magnification, and (c) EDX Mapping of GNS

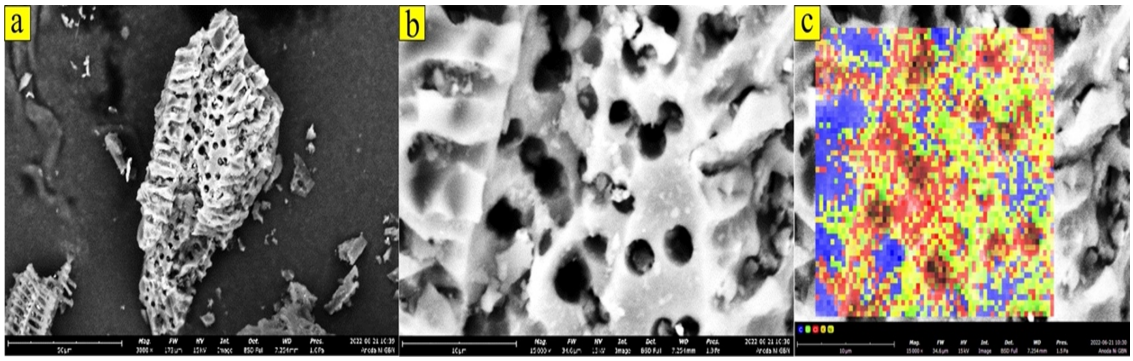

Figure 4. (a) Ni/GNS Morphology at 5000× Magnification, (b) Ni/GNS Morphology at 10,000× Magnification, and (c) EDX Mapping of Ni/GNS

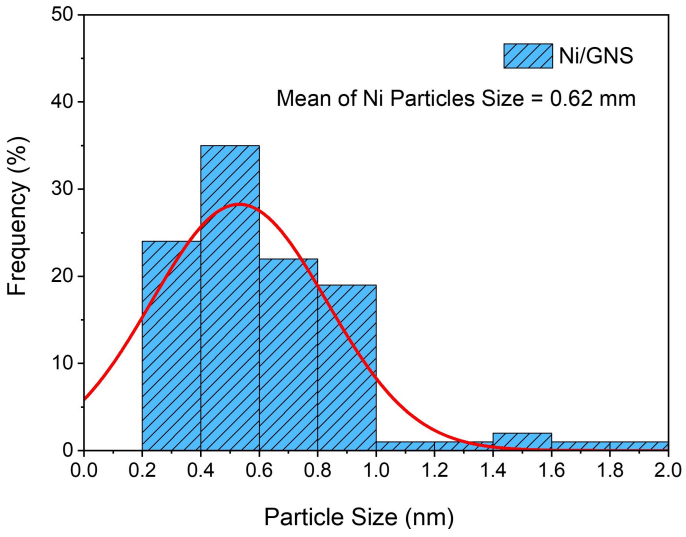

Figure 5. Ni Particle Size Distribution in Ni/GNS

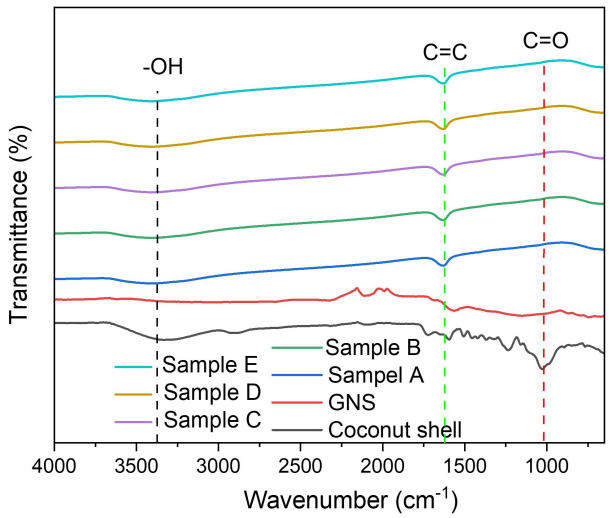

Figure 6. FTIR Characterization of GNS and Electrode samples

The GNS was then modified through the deposition of Ni metal, and the resulting material was characterized using XRD. Figure 2 shows the XRD diffraction pattern of Ni/GNS, with weak and broad peaks at 2θ = 43.51°. This data aligns with the JCPDS 04-850 data (Ali et al., 2022), which states that Ni (200) exhibits peaks at 2θ = 43 - 44.5°. Meanwhile, the weak and broad peak at 24.21°, marked as C (002), indicates the

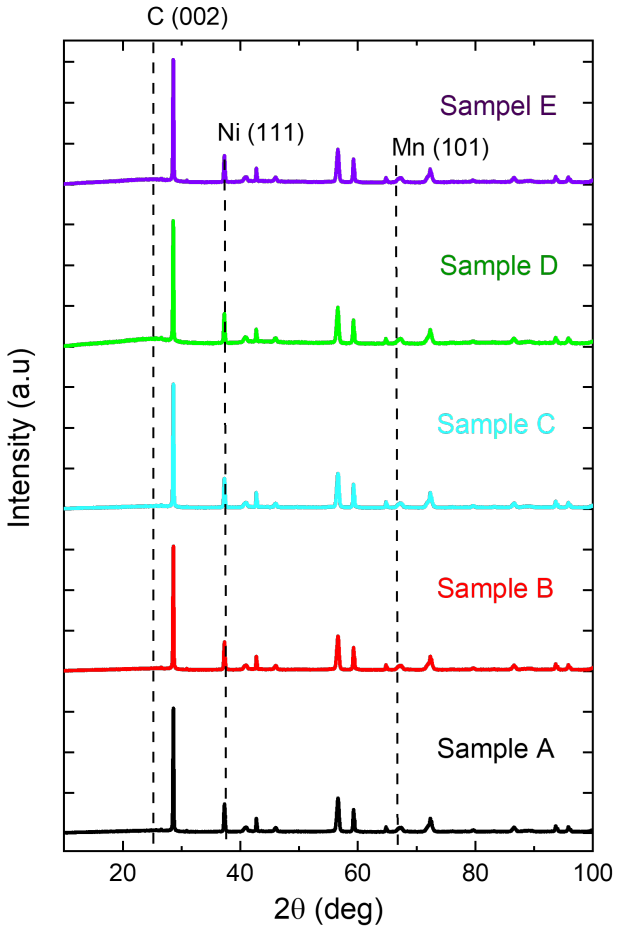

Figure 7. XRD Diffraction Pattern of the Ni/GNS//Electrolyte //GNS Samples

formation of GNS. This suggests that Ni has been successfully deposited onto the GNS, as per JCPDS 75-2078 (Kumar et al., 2020).

3.2 SEM-EDX Analysis of GNS and Ni/GNS

The surface morphology of the GNS characterized by SEM is illustrated in Figures 3(a) and 3(b). These figures show the SEM images of GNS at magnifications of 5000× and 10,000×, respectively. At the 5000× magnification, as seen in Figure 3(a), the morphology of the GNS reveals an uneven surface with irregularly stacked layers. This appearance indicates that the graphene has a layered structure, and the presence of pores is a characteristic feature of layered graphene (Saleh et al., 2022). Meanwhile, Figure 3(b) shows the GNS at a higher magnification of 10,000×, where the surface of GNS consists of neatly arranged and flat carbon layers. The surface of GNS is flat and is composed of randomly stacked layers that are thin (Supeno and Siburian, 2020).

Figure 3(c) shows the mapping results of the GNS material, indicated by the abundance of C and O atoms. Table 1 further presents the EDX data in more detail. The mapping in Figure 3(c) reveals that GNS is predominantly represented by the color blue, which is clarified by EDX data showing that GNS is primarily composed of C atoms (71.50 wt%). Additionally, GNS also contains other elements, as shown in Table 1, with O atoms being the second most abundant at 15.40%, and K atoms the third at 11.30%. The presence of O in this case may be due to the pyrolysis process not completely breaking down all oxygen-containing functional groups (Kong et al., 2020). Furthermore, post-pyrolysis interaction with air can lead to the oxidation of the GNS surface. Meanwhile, Na and K may naturally occur in coconut shell, and during pyrolysis, these non-organic minerals are not decomposed and remain in the final product.

Table 1. Results of EDX Analysis from GNS

	Element	Atomic Concentration	wt%
	C	81.897	71.50
	O	13.241	15.40
	Na	0.478	0.80
	Si	0.098	0.20
	Cl	0.310	0.80
	K	3.976	11.30

The SEM characterization results of Ni/GNS are shown in Figures 4(a) and 4(b), revealing that Ni/GNS has an uneven surface, clearly visible pores, and is dominated by white spots. This indicates that Ni has been successfully deposited on GNS. In addition, Figure 4(c) displays the EDX mapping results for Ni/GNS, which are detailed in Table 2. This shows that Ni/GNS has a high concentration of C atoms (65.10%) and Ni atoms (11.90%). However, the still abundant presence of oxygen (17.60%) may negatively impact the electrical conductivity and energy storage capacity of GNS. Oxygen-containing functional groups can disrupt the ideal graphene structure for electron conduction (Meng et al., 2016). Positively, the oxygen content can boost the interaction between the electrode and the electrolyte, aiding the ion intercalation and deintercalation processes. This enhancement is attributed to the increased electrochemical affinity and wettability of the GNS, which results from the presence of oxygen-containing functional groups (Feng and Guo, 2019). Further analysis of the average particle size of Ni/GNS is presented in Figure 5, showing the Ni particle size in Ni/GNS to be 0.62 μm.

Table 2. Results of EDX Analysis from Ni/GNS

	Element	Atomic Concentration	wt%
	C	78.876	65.10
	O	16.007	17.60
	Cl	1.682	4.10
	K	0.484	1.30
	Ni	2.950	11.90

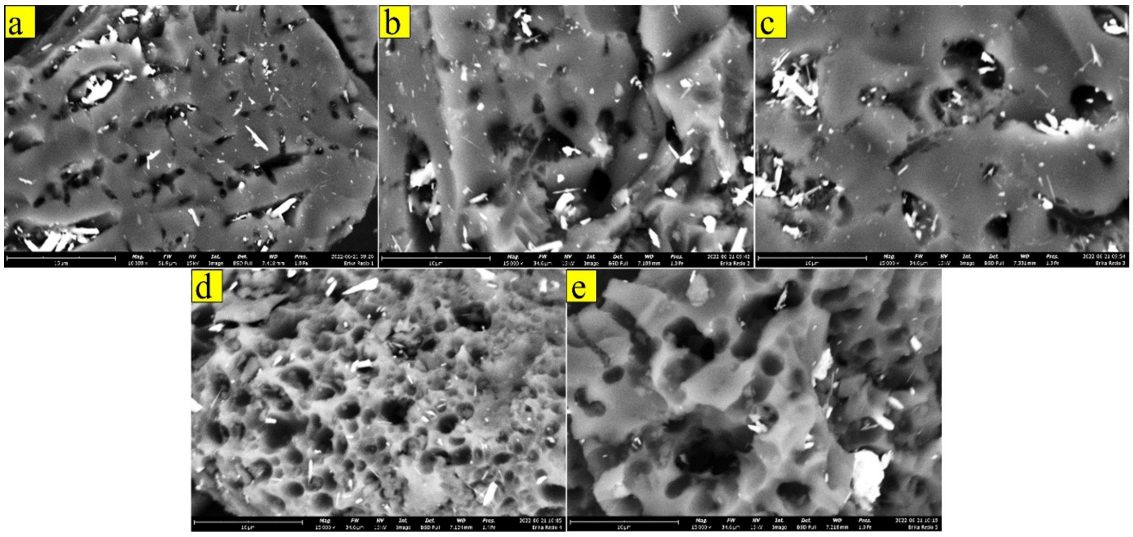

Figure 8. SEM Morphology of Ni/GNS//Electrolyte//GNS at 15,000× Magnification for Samples A, B, C, D, and E

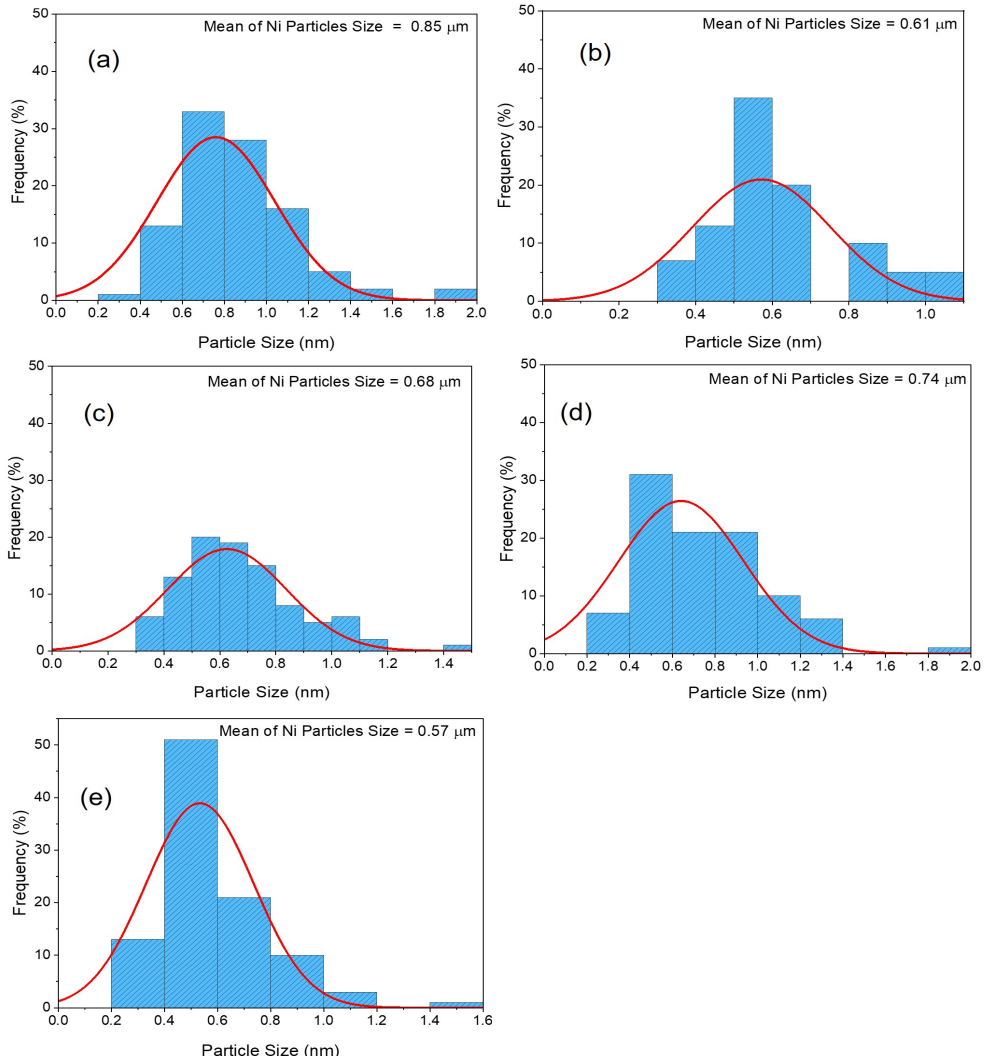

Figure 9. Particle Size Distribution of Ni in Ni/GNS//Electrolyte//GNS Samples (A, B, C, D, and E)

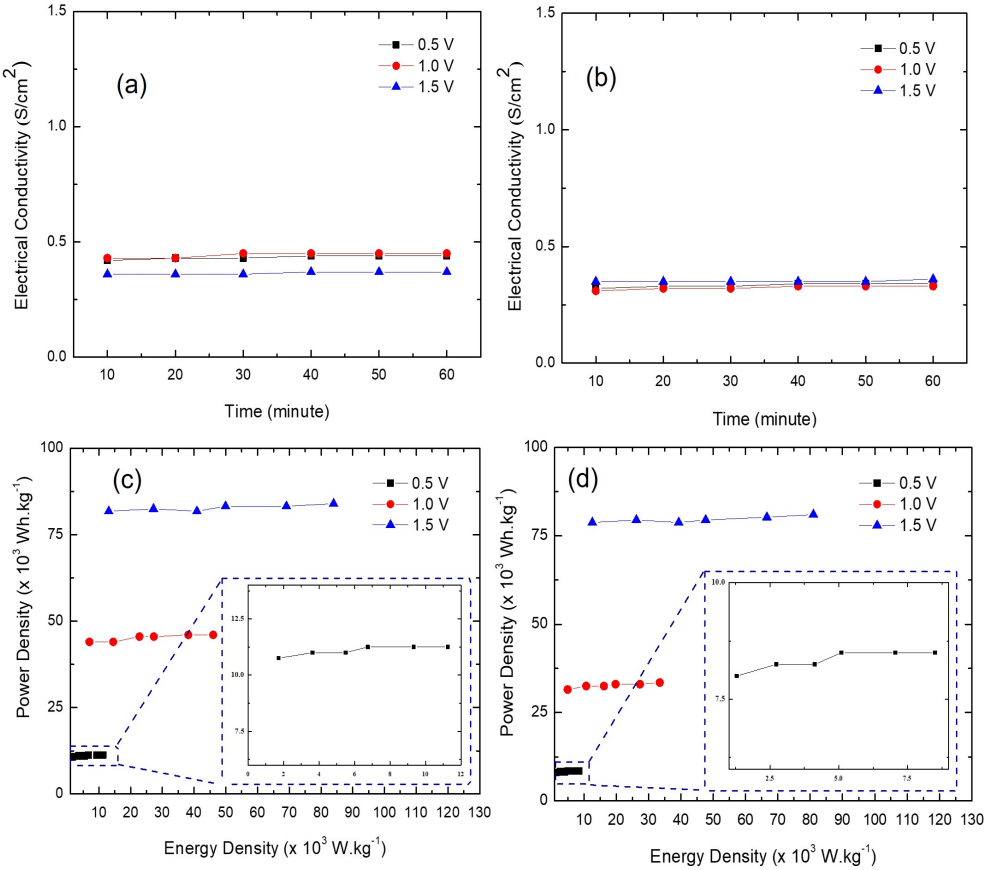

Figure 10. Electrical Conductivity of (a) Commercial Battery Cathode and (b) GNS Cathode, and Battery Performance Testing of (c) Commercial Battery Cathode and (d) GNS Cathode

3.3 Characterization of Ni/GNS//Electrolyte//GNS Sample

FTIR was employed to characterize the functional groups of the electrodes with various sample variations, including GNS and coconut shell, and the results are demonstrated in Figure 6. The peaks of coconut shell at 3348, 2097, 1627, and 1097 cm^{-1} are attributed to −OH, −NH, C=O, and C−O (Ong et al., 2020). After pyrolysis, GNS was synthesized, leading to the appearance of peaks at 1620 cm^{-1}. A peak between 1500 and 1750 cm^{-1} for GNS indicates the presence of C-sp2 aromatic bonds (Baqiya et al., 2020), distinguishing it from coconut shell, suggesting the formation of GNS. Compared to the various sample variations, a shift of peaks from 1627 to 1640 cm^{-1} in the stretching vibrations of Ni bonded with the C=O group can be observed. This suggests that Ni has been successfully deposited onto the GNS (Diantoro et al., 2023). Nevertheless, all sample variations show various functional groups formed, indicating that the performance of carbon-based supercapacitors could be enhanced. Oxygen-containing functional groups such as hydroxyl group (−OH) present in the composite samples can increase the pseudocapacitance of the carbon-based materials as they act as active sites for adsorption and reaction of electrolyte ions (Yang et al., 2015).

The XRD analysis results of Ni/GNS//electrolyte//GNS are shown in Figure 7. The diffraction pattern indicates GNS at a peak of 2θ = 26.00° and Ni at 2θ = 37.21°. Additionally, the diffraction pattern of MnO_2, identified as Mn (220), shows that MnO_2 is deposited on the electrode at 2θ = 65.80° (Otgonbayar et al., 2021).

Figure 8 shows the morphology of Ni/GNS//electrolyte//GNS with various variations. SEM images of sample A, with a Ni/GNS : electrolyte : GNS ratio of 1:2:1, where the mass of the electrolyte is twice that of the anode (Ni/GNS) and cathode (GNS), reveal that the electrode material has irregular pores, a flat surface, and a few small white spots, indicating minimal anode material on the surface. In sample B (2:2:1), where the anode and electrolyte are twice the mass of the cathode, the electrode shows a wrinkled surface with few, irregular pores and is covered with white spots and small patches. For sample C (1:2:2), with the electrolyte and cathode having a greater mass than the anode, the electrode exhibits a flat surface dominated by larger white spots. In sample D (2:1:2), where the cathode and anode have a larger composition than the electrolyte, the surface has larger pores and is dominated by large, white patches. Lastly, sample E (1:1:2), with a larger cathode mass compared to the anode and electrolyte, features few but large pores and some unevenly distributed large white patches.

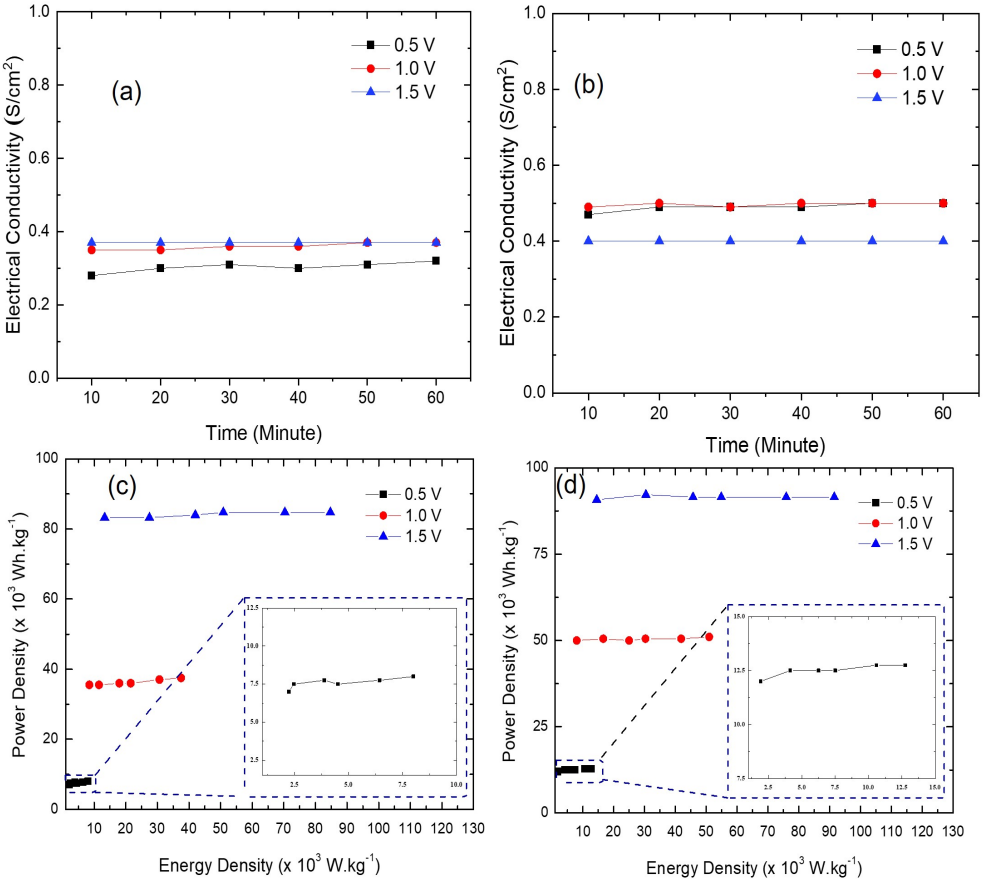

Figure 11. Electrical Conductivity of (a) Commercial Battery anode and (b) Ni/GNS Anode, and Battery Performance Testing of (c) Commercial Battery Anode and (d) Ni/GNS Anode

Among the five samples, sample D has smaller and more regular pores compared to the other four samples. Additionally, the small white spots indicating the presence of Ni on the GNS are well-distributed and uniform in size. This suggests that the Ni/GNS//electrolyte//GNS electrode is well-integrated. The smaller pore size and more uniform distribution contribute to an increased surface area, which is crucial in electrochemical applications. A larger surface area provides more active sites for electrochemical reactions, potentially enhancing the efficiency and performance of the electrode (Mahmood et al., 2022; Takasu and Murakami, 2000). The uniform distribution of Ni is particularly significant as Ni acts as a catalyst in many electrochemical applications. Uniformity in Ni distribution ensures that the reactivity and electrocatalytic performance are consistent across the GNS surface, resulting in a more stable and predictable electrochemical response (Kirubasankar et al., 2018).

EDX analysis of various electrode samples is listed in Table 3. The EDX data show that the elemental abundance is dominated by carbon atoms. The nickel abundance in samples A through E is 0.10%, 0.20%, 0.20%, 2.29%, and 0.20%, respectively. The abundant presence of Ni, as in sample D, offers advantages in terms of efficiency, stability, and electrochemical performance. With a higher Ni abundance, the electrocatalytic activity of the electrode can be enhanced (Lim et al., 2018). This is important in applications where the efficiency and speed of electrochemical reactions are critical, such as in electrolysis or the charging and discharging processes of batteries. Additionally, a more abundant presence of Ni in the electrode can lead to improved electrode conductivity (Wang et al., 2021). The increased Ni content can provide better thermal and chemical stability, reduce electrode degradation over time, and offer longer cycle performance (Casas-Cabanas et al., 2018; Cui and Manthiram, 2023; Dixit et al., 2017; Xie et al., 2019).

Figure 9 shows the results of the particle size distribution analysis of electrode samples. The average particle sizes for samples A through E are 0.85, 0.61, 0.68, 0.74, and 0.57 μm, respectively. The largest particle size is found in sample A, where the electrolyte has the highest composition. The electrolyte plays a role in the particle dispersion process. In sample A, the electrolyte can facilitate the agglomeration of Ni and GNS particles into larger particles due to a non-optimal balance between dispersion and agglomeration. In contrast, in sample E, where GNS is much more abundant compared to other samples, receiving contributions from both the anode and cathode. GNS is known for its thin and flat morphology

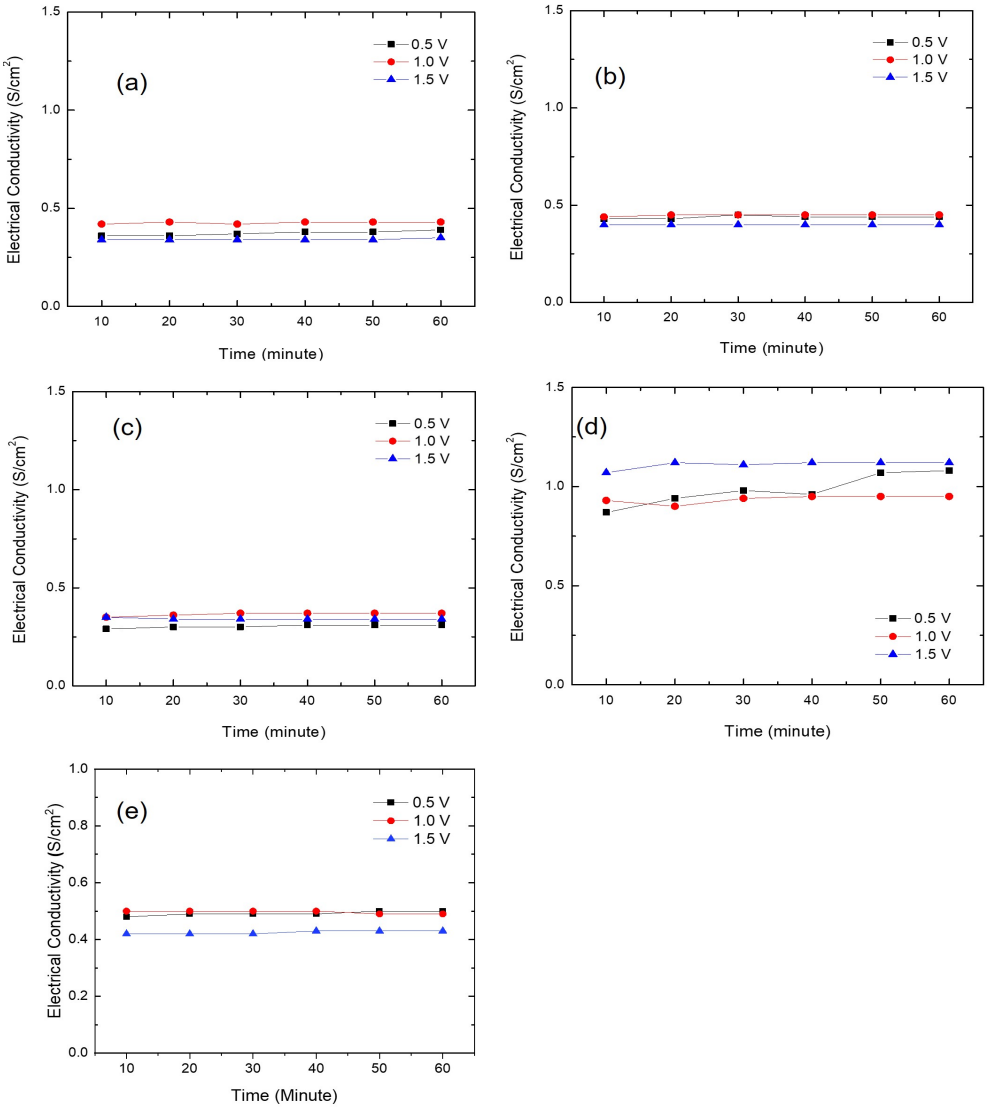

Figure 12. Electrical Conductivity on Prototype Primary Battery

Table 3. Results of EDX Analysis from Ni/GNS//Electrolyte//GNS Samples

Element	wt%				
	A	B	C	D	E
C	90.50	95.00	92.80	91.30	84.11
Ni	0.10	0.20	0.20	2.30	0.20
Mn	6.00	3.30	4.10	3.00	3.40
Cl	3.20	1.50	2.60	3.20	0.60
Si	0.20	NA	0.30	0.20	0.20
O	NA	NA	NA	NA	11.49

Note: NA = Not Available.

(Siburian et al., 2023a). When GNS is present in a dominant amount, it can reduce the overall particle size. GNS can act as a barrier or 'spacer' that prevents the agglomeration of other particles, resulting in a smaller overall particle size distribution (Song et al., 2021).

3.4 Electrical Conductivity Analysis and Battery Performance Testing

Electrical conductivity and performance testing were conducted on various materials, both as anodes and cathodes, and in the form of primary battery fuses. Additionally, commercial batteries were tested to compare their performance with the fabricated batteries. Electrical conductivity was measured by determining the conductance values obtained during tests conducted over durations of 10, 20, 30, 40, and 60 minutes at voltages of 0.5, 1.0, and 1.5 V. The obtained conductance values (S) were then calculated to determine the conductivity in S/cm^2. Meanwhile, battery performance testing involved measuring the energy density (Wh/kg) and power density (W/kg)

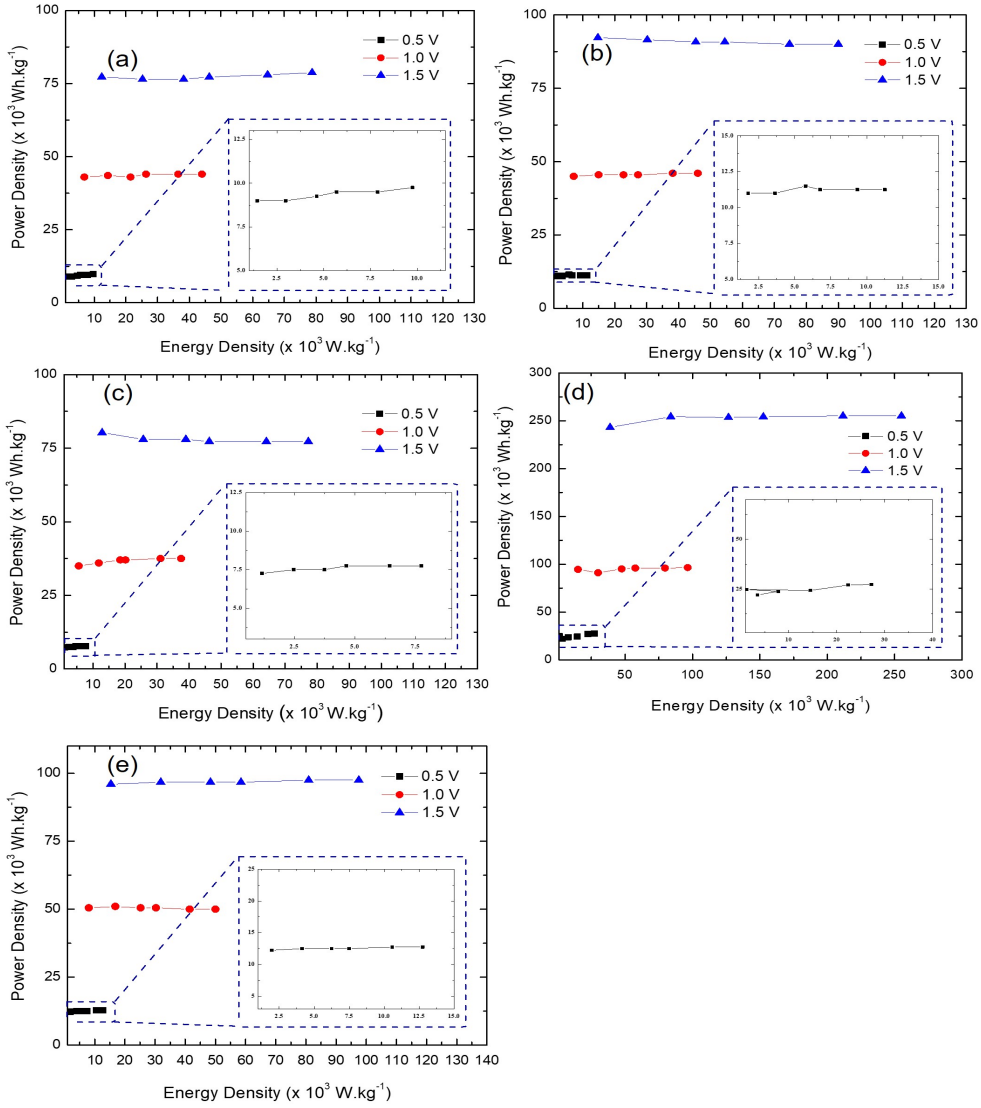

Figure 13. Battery Performance Testing: Energy Density vs. Power Density

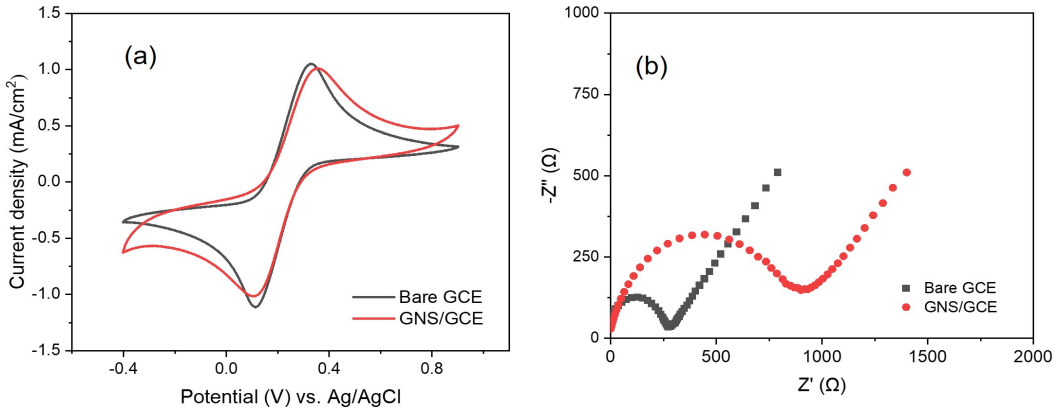

Figure 14. (a) CV Curves and (b) EIS Results of Bare GCE and GNS/GCE Recorded in 0.1M KCl Containing 5 mM $[Fe(CN)_6]^{3-/4-}$

Table 4. Comparison of Energy and power Density with Previous Studies

Electrode	Energy density (Wh/kg)	Power density (W/kg)	References
Ni-Al LDH/nitramine-N-doped graphene	59	1991	(Tian et al., 2018)
Al doped Co hydroxyl fluoride nanosheets	42.7	382.6	(Wang et al., 2019)
NiCoMn-LDH	53.55	448.3	(He et al., 2023)
Activated carbon and nickel-silicon composite	NA	92.64	(Diantoro et al., 2023)
Ni/GNS and GNS	144,788	252,500	This work

Note: NA = Not Available.

at voltages of 0.5, 1.0, and 1.5 V. The purpose of measuring electrical conductivity was to evaluate how efficiently ions can move through the electrolyte and how effectively electrons can flow through the current collector and electrodes. The measurement of energy density aimed to determine how quickly the battery can deliver its maximum power. The measurement of power density was intended to assess how long the battery can operate before needing to be recharged or replaced.

3.4.1 Cathode Testing

The results of the electrical conductivity and battery cathode performance testing analysis can be seen in Figure 10. Commercial primary battery cathodes produced an average electrical conductivity of 0.36 S/cm^2, whereas the electrical conductivity measurement for the GNS cathode was 0.35 S/cm^2 (Figure 10(a) and 10(b)). According to Figure 10(c) and 10(d), it was found that the average energy density and power density of the commercial cathode were 45,586 Wh/kg and 81,000 W/kg, respectively, while the prototype cathode exhibited 45,586 Wh/kg and 79,625 W/kg, respectively.

Based on this analysis, the commercial cathode shows slightly better performance in terms of electrical conductivity and power density, while both cathodes are equivalent in terms of energy density. However, the differences are not significant, especially in terms of electrical conductivity and power density. This indicates that the prototype cathode performs nearly on par with the commercial cathode, which is impressive considering it is a prototype. This can be attributed to the hexagonal structure of graphene, which allows for high charge mobility and a large surface area (Siburian et al., 2023b), resulting in high energy and power densities. Therefore, GNS synthesized from coconut fruit has potential as a supporting material in primary battery cells.

3.4.2 Anode Testing

Figure 11 shows the results of electrical conductivity testing and battery performance testing for a commercial battery anode and a Ni/GNS anode. The average electrical conductivity values for the two anodes are 0.40 S/cm^2 for the commercial battery anode and 0.37 S/cm^2 for the Ni/GNS anode. In Figures 11(c) and 11(d), it is shown that the average energy density for the commercial battery anode is 48,112 Wh/kg, and for the Ni/GNS anode, it is 48,123 Wh/kg, while the average power density for both the commercial battery anode and the Ni/GNS anode is the same at 84,125 W/kg. These results indicate that both the commercial battery anode and the Ni/GNS anode are capable of oxidizing ions effectively. The testing results presented suggest that both the commercial battery anode and the Ni/GNS anode demonstrate very similar performance in oxidizing ions, which is important for the efficiency of electrochemical reactions in batteries.

3.4.3 Primary Battery Prototype Testing

The results of the electrical conductivity testing on the prototype primary battery with the Ni/GNS//electrolyte//GNS cell are shown in Figure 12. The average electrical conductivity values for the various sample variations from A to E are 0.34, 0.40, 0.34, 1.11, and 0.43 S/cm^2, respectively. Consequently, it is concluded that sample D has the highest efficiency in electrical conductivity. This is influenced by the equal ratio of anode to cathode, specifically a Ni/GNS : electrolyte : GNS ratio of 2:1:2, resulting in a greater oxidation charge from the anode and a larger reduction charge by the cathode, thereby generating a larger current. With a higher Ni/GNS ratio compared to other samples, it is possible that the distribution of Ni/GNS and GNS within the electrode matrix is more homogeneous.

The analysis of energy density and power density in the prototype primary battery is shown in Figure 13. The average energy density values for samples A-E are 44,282; 51,580; 44,216; 144,788; and 55,431 Wh/kg, respectively. Notably, sample D stands out with an energy density of 144,788 Wh/kg, significantly higher than the other samples. This indicates that sample D can store more energy per unit mass compared to the other samples, a highly desirable characteristic in battery applications, especially for applications requiring efficient and lightweight energy storage. Meanwhile, the average power densities for samples A-E are 77,375; 90,875; 78,000; 252,500; and 97,000 W/kg, respectively. Sample D has the highest power density at 252,500 W/kg, indicating the battery's ability to produce a large amount of power relative to its mass. This is important in applications that require high levels of energy discharge in a short period, such as in applications needing rapid response or high power. The data obtained show that the energy density and power density of a material are related to the magnitude of electrical power and the cross-sectional area of the medium used in conducting electricity. The greater

the electrical power used, the larger the resulting power density (Krawczyk et al., 2019). From this data, it can be concluded that sample D has the best performance in terms of both energy density and power density, making it a highly promising candidate for primary battery applications with high energy and power requirements.

The current electrode material displayed highly competitive performance compared to previously reported research. According to Table 4, the combination of Ni/GNS with GNS exhibited significantly elevated energy and power density metrics compared to earlier studies. This indicates that the Ni/GNS //electrolyte//GNS configuration holds considerable promise as a primary battery material.

3.5 Electrical Measurement of GNS

The electrochemical performance of GNS was evaluated on GNS/GCE. CV curves in Figure 14(a) demonstrate the redox behavior of the prepared electrodes in 0.1 M KCl containing 5 mM $[Fe(CN)_6]^{3-/4-}$.

Based on CV curves obtained from the redox probe $[Fe(CN)_6]^{3-/4-}$, the greatest current response was recorded on bare GCE, followed by GNS/GCE (Figure 14a). According to the Nyquist plots (Figure 14b), the charge transfer resistance (Rct) of bare GCE and GNS/GCE were 0.30 kΩ and 0.88 kΩ, respectively. This value can significantly change by combining GNS with metals or conductive polymers, indicating that the CV and EIS results were consistent, showing that GNS may transport electrons due to its electrical conductivity.

4. CONCLUSIONS

The results of the study on the effect of mass ratio in the anode: electrolyte: cathode composition indicate that the combination of Ni/GNS and GNS shows potential as an electrode for primary batteries. This is evident from the average electrical conductivity values produced by samples A to E, which are 0.34, 0.40, 0.34, 1.11, and 0.43 S/cm^2, respectively. Furthermore, the battery performance testing supports these findings on electrical conductivity, demonstrating that sample D has the best performance among the samples. This is evidenced by its energy density and power density values, which are 144,788 Wh/kg and 252,500 W/kg, respectively. Moreover, the data obtained from CV and EIS exhibited coherence, with resistance values of 0.30 kΩ and 0.88 kΩ, suggesting the potential of GNS to facilitate electron conduction due to its inherent electrical conductivity.

5. ACKNOWLEDGMENT

The authors wish to express their gratitude to the Analytical Chemistry Laboratory and the Physics Laboratory of Universitas Sumatera Utara, as well as the Laboratory of Universitas Pertahanan Jakarta, for providing research facilities and instrumental analysis support.

REFERENCES

Alessia, A., B. Alessandro, V. Maria, V. Carlos, and B. Francesca (2021). Challenges for Sustainable Lithium Supply: A Critical Review. *Journal of Cleaner Production*, **300**; 126954

Ali, M. J. M., M. M. Radhy, and E. M. Ali (2022). Synthesis and Characterization of Copper Oxide Nanoparticles and Their Application for Solar Cell. *Materials Today: Proceedings*, **60**; 917–921

An, X., C. Liu, J. Liu, J. Liu, and Y. Liu (2024). Reconstructing Hydrogen Bond Network with Chaotropic Salt Enables Low-Temperature and Long-Life Nickel-Zinc Batteries. *Journal of Power Sources*, **596**; 234096

Baqiya, M. A., A. Y. Nugraheni, W. Islamiyah, A. F. Kurniawan, M. M. Ramli, S. Yamaguchi, Y. Furukawa, S. Soontaranon, E. G. R. Putra, and Y. Cahyono (2020). Structural Study on Graphene-Based Particles Prepared from Old Coconut Shell by Acid–Assisted Mechanical Exfoliation. *Advanced Powder Technology*, **31**(5); 2072–2078

Casas-Cabanas, M., M. D. Radin, J. Kim, C. P. Grey, A. Van der Ven, and M. R. Palacín (2018). The Nickel Battery Positive Electrode Revisited: Stability and Structure of the β-Niooh Phase. *Journal of Materials Chemistry A*, **6**(39); 19256–19265

Chameh, B., M. H. Saznaghi, T. Shahalizade, S. Javanmardi, H. Samandari, M. Molababaei, B. Raissi, A. Aghaei, M. S. Yaghmaee, and R. Riahifar (2024). Electrophoretic Deposition of Graphene Oxide As a Stabilizing Layer on the Ni-Rich Layered Oxide Electrodes for Enhancing the Cycling Stability of Li-Ion Cathodes. *Journal of Energy Storage*, **81**; 110415

Chang, J., Z. Hu, J. Li, D. Wu, Z. Lian, F. Xu, K. Jiang, and Z. Gao (2021). Ultrathin NiAl Layered Double Hydroxide-Reduced Graphene Oxide Composite Nanosheets Array with High Battery Performances for Hybrid Supercapacitor and Hybrid Battery. *Applied Surface Science*, **538**; 148106

Chen, X., Y. Jia, Z. Shi, Q. Le, J. Li, M. Zhang, M. Liu, and A. Atrens (2021a). Understanding the Discharge Behavior of an Ultra-High-Purity Mg Anode for Mg–Air Primary Batteries. *Journal of Materials Chemistry A*, **9**(37); 21387–21401

Chen, X., X. Liu, Q. Le, M. Zhang, M. Liu, and A. Atrens (2021b). A Comprehensive Review of the Development of Magnesium Anodes for Primary Batteries. *Journal of Materials Chemistry A*, **9**(21); 12367–12399

Cui, Z. and A. Manthiram (2023). Thermal Stability and Outgassing Behaviors of High-Nickel Cathodes in Lithium-Ion Batteries. *Angewandte Chemie International Edition*, **62**(43); e202307243

Dahal, A. and M. Batzill (2014). Graphene–Nickel Interfaces: A Review. *Nanoscale*, **6**(5); 2548–2562

Diantoro, M., I. Istiqomah, O. P. D. Lestari, Y. Al Fath, Y. Yudyanto, C. I. Yogihati, M. Munasir, D. H. Kusumawati, and Z. B. Aspanut (2023). A Comprehensive Study of

Binder Polymer for Supercapattery Electrode Based on Activated Carbon and Nickel-Silicon Composite. *Materials Science for Energy Technologies*, **6**; 368–381

Dixit, M., B. Markovsky, F. Schipper, D. Aurbach, and D. T. Major (2017). Origin of Structural Degradation during Cycling and Low Thermal Stability of Ni-Rich Layered Transition Metal-Based Electrode Materials. *The Journal of Physical Chemistry C*, **121**(41); 22628–22636

Feng, J. and Z. Guo (2019). Wettability of Graphene: From Influencing Factors and Reversible Conversions to Potential Applications. *Nanoscale Horizons*, **4**(2); 339–364

Ha, S., C. Lim, and Y.-S. Lee (2022). Fluorination Methods and the Properties of Fluorinated Carbon Materials for Use As Lithium Primary Battery Cathode Materials. *Journal of Industrial and Engineering Chemistry*, **111**; 1–17

He, L., G. Wang, N. u. R. Lashari, Z. Guo, and M. Li (2023). Polypyrrole-Derived Carbon Coated NiCoMn Layered Double Hydroxides for High-Performance Supercapacitors. *ACS Applied Nano Materials*, **6**(18); 16400–16413

Hu, X., L. Xu, X. Lin, and M. Pecht (2020). Battery Lifetime Prognostics. *Joule*, **4**(2); 310–346

Kirubasankar, B., V. Murugadoss, J. Lin, T. Ding, M. Dong, H. Liu, J. Zhang, T. Li, N. Wang, and Z. Guo (2018). In Situ Grown Nickel Selenide on Graphene Nanohybrid Electrodes for High Energy Density Asymmetric Supercapacitors. *Nanoscale*, **10**(43); 20414–20425

Kong, X., Y. Zhu, H. Lei, C. Wang, Y. Zhao, E. Huo, X. Lin, Q. Zhang, M. Qian, and W. Mateo (2020). Synthesis of Graphene-Like Carbon from Biomass Pyrolysis and Its Applications. *Chemical Engineering Journal*, **399**; 125808

Krawczyk, P., B. Gurzęda, and A. Bachar (2019). Thermal Exfoliation of Electrochemically Obtained Graphitic Materials. *Applied Surface Science*, **481**; 466–472

Kumar, R., S. Sahoo, E. Joanni, R. K. Singh, K. Maegawa, W. K. Tan, G. Kawamura, K. K. Kar, and A. Matsuda (2020). Heteroatom Doped Graphene Engineering for Energy Storage and Conversion. *Materials Today*, **39**; 47–65

Lee, S., J. Hwang, C. Park, S. Ahn, K. Do, S. Kim, and H. Ahn (2023). Efficient and Scalable Encapsulation Process of Highly Conductive 1T-MoS_2 Nanosheets on Ni-Rich $LiNi_{0.83}Co_{0.11}Mn_{0.06}O_2$ Cathode Materials for High-Performance Lithium-Ion Batteries. *Chemical Engineering Journal*, **470**; 144209

Lim, K. J. H., G. Yilmaz, Y.-F. Lim, and G. W. Ho (2018). Multi-compositional Hierarchical Nanostructured Ni_3S_2@MoSx/NiO Electrodes for Enhanced Electrocatalytic Hydrogen Generation and Energy Storage. *Journal of Materials Chemistry A*, **6**(41); 20491–20499

Mahmood, M., S. Zulfiqar, M. F. Warsi, M. Aadil, I. Shakir, S. Haider, P. O. Agboola, and M. Shahid (2022). Nanostructured V_2O_5 and Its Nanohybrid with Mxene As an Efficient Electrode Material for Electrochemical Capacitor Applications. *Ceramics International*, **48**(2); 2345–2354

Manalu, A., K. Tarigan, S. Humaidi, M. Ginting, K. Sebayang, M. Rianna, M. Hamid, A. Subhan, P. Sebayang, and I. P. Manalu (2022). Synthesis, Microstructure and Electrical Properties of $NiCo_2O_4$/rGO Composites as Pseudocapacitive Electrode for Supercapacitors. *International Journal of Electrochemical Science*, **17**(3); 22036

Meng, Q.-L., H.-C. Liu, Z. Huang, S. Kong, X. Lu, P. Tomkins, P. Jiang, and X. Bao (2016). Mixed Conduction Properties of Pristine Bulk Graphene Oxide. *Carbon*, **101**; 338–344

Moulai, F., B. Messaoudi, L. Zerroual, T. Hadjersi, and A. Achour (2020). Assembled Manganese and Its Nanostructured Manganese Dioxide Rich Electrodes for a New Primary Battery. *Materials Chemistry and Physics*, **244**; 122717

Murata, H., Y. Nakajima, N. Saitoh, N. Yoshizawa, T. Suemasu, and K. Toko (2019). High-Electrical-Conductivity Multilayer Graphene Formed by Layer Exchange with Controlled Thickness and Interlayer. *Scientific reports*, **9**(1); 4068

Ong, H. C., W. Chen, Y. Singh, Y. Y. Gan, C. Chen, and P. L. Show (2020). A State-Of-The-Art Review on Thermochemical Conversion of Biomass for Biofuel Production: A TG-FTIR Approach. *Energy Conversion and Management*, **209**; 112634

Otgonbayar, Z., K. N. Fatema, S. Yang, I. Kim, M. Kim, S. E. Shim, and W. Oh (2021). Temperature Dependence for High Electrical Performance of Mn-Doped High Surface Area Activated Carbon (HSAC) As Additives for Hybrid Capacitor. *Scientific Reports*, **11**(1); 534

Porzio, J. and C. D. Scown (2021). Life-Cycle Assessment Considerations for Batteries and Battery Materials. *Advanced Energy Materials*, **11**(33); 2100771

Reyes, C., R. Somogyi, S. Niu, M. A. Cruz, F. Yang, M. J. Catenacci, C. P. Rhodes, and B. J. Wiley (2018). Three-Dimensional Printing of a Complete Lithium Ion Battery with Fused Filament Fabrication. *ACS Applied Energy Materials*, **1**(10); 5268–5279

Saleh, A., F. A. Amhadin, and I. Novianty (2022). Synthesis of Reduced Graphene Oxide and Zinc Oxide Composite from Candlenut Shell Charcoal (*Aleuritas moluccana*). *Elkawnie: Journal of Islamic Science and Technology*, **8**(1); 1–11

Sayahpour, B., H. Hirsh, S. Bai, N. B. Schorr, T. N. Lambert, M. Mayer, W. Bao, D. Cheng, M. Zhang, and K. Leung (2022). Revisiting Discharge Mechanism of CFx As a High Energy Density Cathode Material for Lithium Primary Battery. *Advanced Energy Materials*, **12**(5); 2103196

Siburian, R., R. Goei, H. Manurung, S. P. Aritonang, C. Simanjuntak, F. Hutagalung, I. Anshori, Y. Alias, S. Paiman, and J. Affi (2023a). Distribution Model of Iron (Fe) on Fe/graphene Nano Sheets. *Ceramics International*, **49**(17); 28571–28579

Siburian, R., F. Hutagalung, O. Silitonga, S. Paiman, L. Simatupang, C. Simanjuntak, S. P. Aritonang, Y. Alias, L. Jing, and R. Goei (2023b). The New Materials for Battery Electrode Prototypes. *Materials*, **16**(2); 555

Siburian, R., S. Paiman, F. Hutagalung, L. Simatupang, R. Goei, and M. M. Rusop (2022). Developing Nickel/Graphene Nano Sheets As an Alternative Primary

Battery Anode. *Ceramics International*, **48**(9); 12897–12905

Siburian, R. and O. Silitonga (2022). Performance of Primary Battery Prototype: Cu/Graphene Nano Sheets//Electrolyte//C-π (Graphite, Graphene Nano Sheets, N–Graphene Nano Sheets). In *AIP Conference Proceedings*, volume 2638. AIP Publishing

Siburian, R., L. W. Tang, Y. Alias, A. I. Y. Tok, R. Goei, C. Simanjuntak, K. Tarigan, S. Paiman, B. T. Goh, and I. Anshori (2023c). Coconut Waste to Green Nanomaterial: Large Scale Synthesis of N-Doped Graphene Nano Sheets. *Nano-Structures & Nano-Objects*, **36**; 101061

Song, Z., C. Zhang, X. Fu, H. Zhang, J. Xian, and J. Lin (2021). Graphene Nanosheet As a New Particle Dispersant for the Jet-Electrodeposition of High-Performance Ni-P-WC Composite Coatings. *Surface and Coatings Technology*, **425**; 127740

Sookhakian, M., G. B. Tong, and Y. Alias (2020). In-Situ Electrodeposition of Rhodium Nanoparticles Anchored on Reduced Graphene Oxide Nanosheets As an Efficient Oxygen Reduction Electrocatalyst. *Applied Organometallic Chemistry*, **34**(3); e5370

Sun, B., W. Tang, H. Xiang, W. Xu, Y. Cong, G. Yuan, H. Zhu, Q. Zhang, and X. Li (2022). Improving Electron and Ion Transport by Constructing 3D Graphene Nanosheets Sandwiched between Porous Carbon Nanolayers Produced from Resorcinol-Formaldehyde Resin for High-Performance Supercapacitor Electrodes. *New Carbon Materials*, **37**(3); 564–574

Supeno, M. and R. Siburian (2020). New Route: Convertion of Coconut Shell Tobe Graphite and Graphene Nano Sheets. *Journal of King Saud University-Science*, **32**(1); 189–190

Takasu, Y. and Y. Murakami (2000). Design of Oxide Electrodes with Large Surface Area. *Electrochimica Acta*, **45**(25-26); 4135–4141

Tian, H., W. Bao, Y. Jiang, L. Wang, L. Zhang, O. Sha, C. Wu, and F. Gao (2018). Fabrication of Ni-Al LDH/Nitramine-N-Doped Graphene Hybrid Composites Via a Novel Self-Assembly Process for Hybrid Supercapacitors. *Chemical Engineering Journal*, **354**; 1132–1140

Wan, S., L. Jiang, and Q. Cheng (2020). Design Principles of High-Performance Graphene Films: Interfaces and Alignment. *Matter*, **3**(3); 696–707

Wang, M., P.-L. Tremblay, and T. Zhang (2021). Optimizing the Electrical Conductivity of Polyacrylonitrile/polyaniline with Nickel Nanoparticles for the Enhanced Electrostimulation of Schwann Cells Proliferation. *Bioelectrochemistry*, **140**; 107750

Wang, Z., J. Chang, L. Chen, Y. Li, D. Wu, F. Xu, K. Jiang, and Z. Gao (2019). Al Doped Co Hydroxyl Fluoride Nanosheets Arrays As Efficient Faradaic Electrode for Hybrid Supercapacitor. *Electrochimica Acta*, **323**; 134815

Wei, Z., J. Cheng, R. Wang, Y. Li, and Y. Ren (2021). From Spent Zn–MnO_2 Primary Batteries to Rechargeable Zn–MnO_2 Batteries: A Novel Directly Recycling Route with High Battery Performance. *Journal of Environmental Management*, **298**; 113473

Xie, S., J. Gou, B. Liu, and C. Liu (2019). Nickel-Cobalt Selenide As High-Performance and Long-Life Electrode Material for Supercapacitor. *Journal of Colloid and Interface Science*, **540**; 306–314

Yang, W., M. Ni, X. Ren, Y. Tian, N. Li, Y. Su, and X. Zhang (2015). Graphene in Supercapacitor Applications. *Current Opinion in Colloid & Interface Science*, **20**(5-6); 416–428

Zou, Q., Q. Le, X. Chen, Y. Jia, C. Ban, T. Wang, H. Wang, R. Guo, L. Ren, and A. Atrens (2022). The Influence of Ga Alloying on Mg-Al-Zn Alloys as Anode Material for Mg-air Primary Batteries. *Electrochimica Acta*, **401**; 139372

